

# Design of magneto-rheological (MR) valve

A. Grunwald and A. G. Olabi

Dublin City University, School of Mechanical and Manufacturing Engineering, Glasnevin,  
Dublin 9, Ireland, Email: [abdul.olabi@dcu.ie](mailto:abdul.olabi@dcu.ie), [artur.grunwald@dcu.ie](mailto:artur.grunwald@dcu.ie)

## Abstract:

Magneto-Rheological Fluid (“MRF”) technology has been successfully employed in various low and high volume automotive applications. Good understanding of specific design constraints is required to define and to optimize a magneto-rheological device. This article presents parametrical analyses with magnetic simulations, of a magneto-rheological valve and a magneto-rheological orifice. Experimental rig assemblies of two different control devices have been designed, built and the performances have been evaluated experimentally.

Controlled pressure drops, of 0.6MPa @ 4.5A at 5cm<sup>3</sup>/s in the orifice mode, and 1.5MPa @ 4.5A at 0 cm<sup>3</sup>/s, in the valve mode, using MRF132-AD, have been achieved. The study shows that excellent features like the fast response and the contactless nature of MRF control are attractive for various control devices.

**Keywords:** Magneto-Rheological Fluid, MRF-valve, MRF-orifice, FEM.

## **1. Introduction of magnetorheological (“MR”) technology**

Magnetorheology (“MR”) is the change of rheological behavior under an external magnetic field. The external magnetic field forces the ferromagnetic particles to form a chain-like structure [6], which resists the free fluid motion, and the fluid behavior becomes controllable with the external magnetic field. The rheological status changes reversibly from liquid to the solid. For most liquids, the viscosity changes only with different chemical compositions, shear stresses and temperatures. The change of viscosity with external magnetic field is the basic feature of MRF technology. The MRF effect is the difference between rheological properties with and without a magnetic field.

There are basically three components in an MR fluid: basic fluid, metal particles and stabilizing additives [1-8, 13, 14]. The base fluid has the function of the carrier and naturally combines lubrication and damping features. For the highest MRF effect the viscosity of the fluid should be small and almost independent of temperature. In this way the MRF effect will be the dominant effect when it is compared with the natural physical viscosity varying with temperature and shear stress. In the off-state (without a magnetic field) MRF’s behave like the base fluid in accordance with their chemical compositions. There are different types of liquid which can be used as the carrier fluid i.e. hydrocarbon oils, mineral oils or silicon oils. The base fluid will have a higher viscosity when the concentration of metal particles is very high, and the fluid will appear to be “thicker” [7]. In the on-state (with a magnetic field) the metal particles are guided by the magnetic field to form a structure. The MR-effect is produced because of the resistance to flow which is caused by the chain-like structure.

The metal particles are usually made of carbonyl iron, or powder iron, or iron / cobalt alloys to achieve a high magnetic saturation. The amount of metal powder in MRF can be up to 50% by volume [1-8]. The particle size is some  $\mu$ -meters and varies depending on the manufacturing processes. In the case of carbonyl iron the particle size is between 1 to 10  $\mu$ -meter. The material specification, especially the permeability is also a very important factor for controlling of the MR-effect.

The additives include stabilizers and surfactants [10]. Additives are suspending agents, thixotropes, friction modifiers and anti-corrosion/wear components. Highly viscous materials such as grease or other thixotropic additives are used to improve stability by hindering setting [11]. Ferrous naphthanate or ferrous oleate can be used as dispersants and metal soaps such as lithium stearate or sodium stearate as thixotropic additives [12]. Additives are required to control the viscosity of the liquid and the settling of the particles, the friction between the

particles and to avoid thickening which occurs as the result of long term usage of the fluid. The total density depends on the formulation and is approximately by 3-4g/cc. All three components define the magneto-rheological behaviour of the MR fluid. The change of one of the MRF components will lead to rheological changes (in the off-state) and to magneto-rheological changes in behaviour (in the on-state). Finally a trade-off between the achievable performances of all three components in combination is required in order to optimize a formulation. The rheological behavior of the MRF is dependent on the chemical formulation and the stability of the chain-like structure, which the fluid has to flow around. The physical background for the MR-effect is depicted with simplification schematically in Fig. 1.

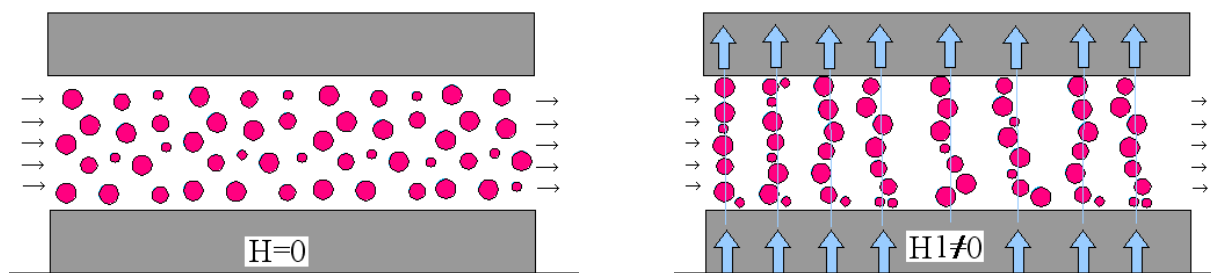


Fig. 1: “MR”-effect, schematically

Without the external magnetic field, the magnetorheological fluid behaves like Newtonian fluid. During the last few years the stability, sedimentation and abrasive behavior have been studied in several universities and companies in the USA, Europe, and Japan. Recently MRF applications such as dampers, clutches, active bearings have already come to the market or are close to the start for high volume production.

## 2. MRF valve and orifice layout

Two different types of control arrangements have been evaluated, the MRF control valve and the MRF control orifice. In case of MRF control valve, the direction of the fluid flow is perpendicular to the external magnetic field. The external magnetic field causes chain-like structures of the MRF particles to form in the gap area. The resistance to flow caused by the particle-structure for the fluid to pass is the reason for the magneto-rheological pressure drop. Fig. 2 shows a cross-section of the MRF control valve. Main assembly components are: coil, housing and internal shaft with attachments. Fig. 3 depicts the flow direction and the orientation of the magnetic field in the gap area.

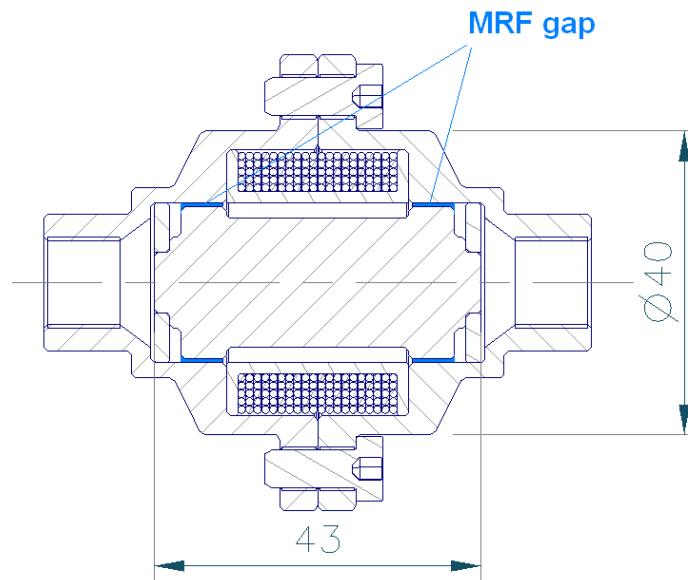


Fig. 2: MRF control valve

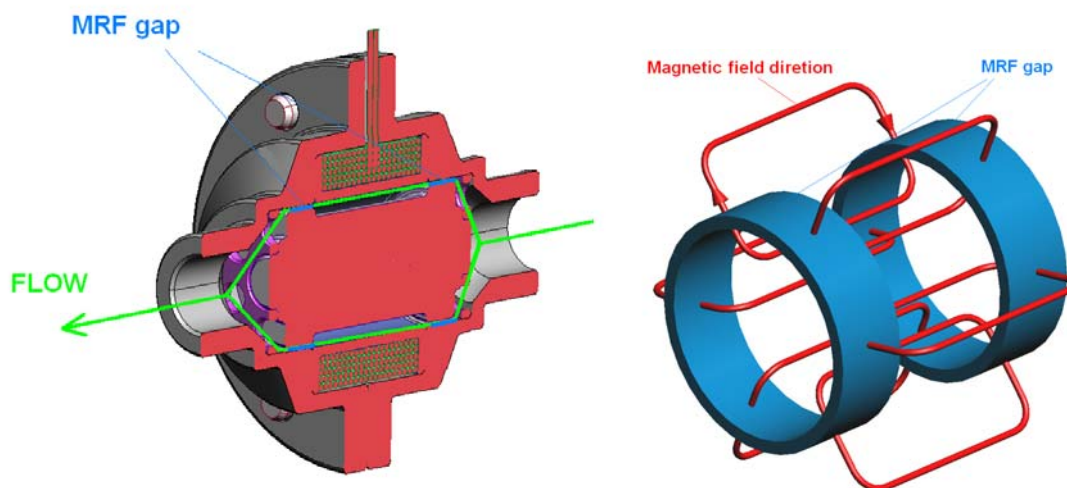


Fig. 3: Fluid flow and magnetic field directions in the valve gap

In the case of the MRF control orifice, the direction of the fluid flow is parallel to the external magnetic field. Fig. 4 shows a cross-section of the MRF control orifice. The external magnetic field causes chain-like structures of the MRF particles in the orifice area. The resistance of particle-structure for the fluid to pass is the reason for the magneto-rheological pressure drop. Main assembly components are: coil and housing with attachments. The coil bobbin inner diameter was designed to be equal to the orifice diameter. Fig. 5 depicts the flow direction and the orientation of the magnetic field in the orifice area.

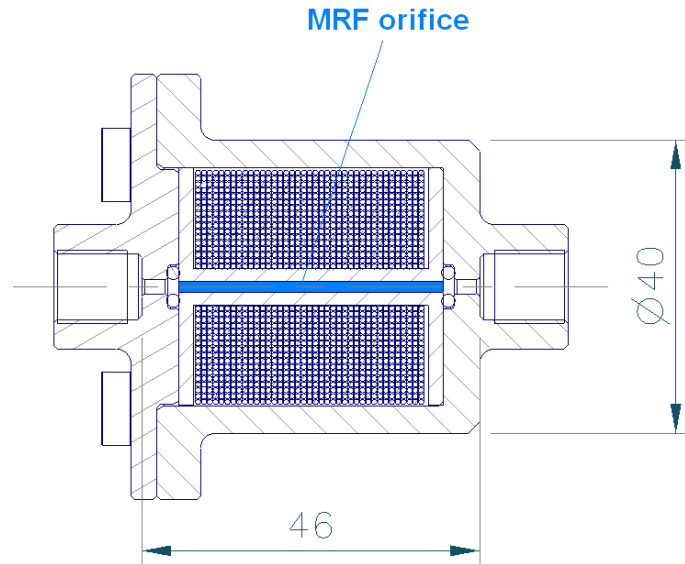


Fig. 4: MRF control orifice

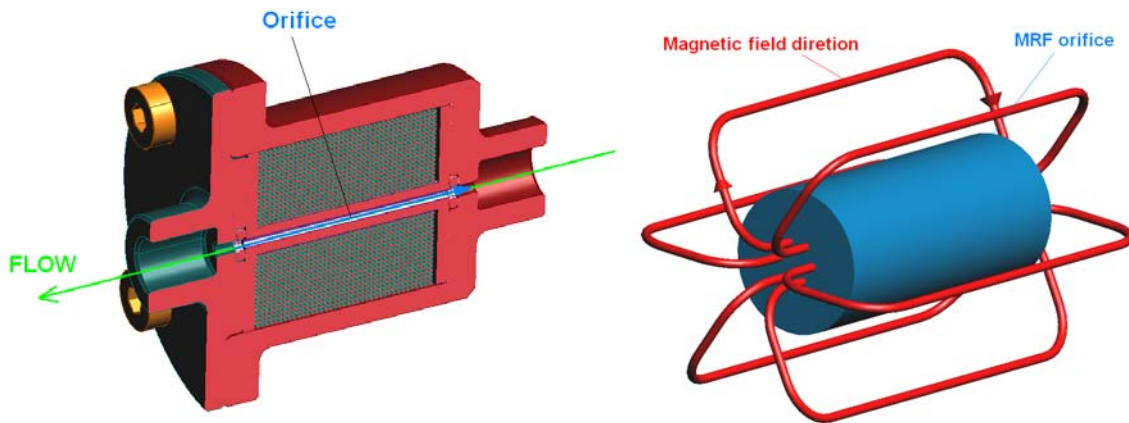


Fig. 5: Fluid flow and magnetic field directions in the orifice

The MRF effect in both layouts has been evaluated theoretically and experimentally. In this study, two fluids MRF-132-AD and MRF-336-AG have been used. The yield stress is the magnetic field dependent rheological feature of the MRF. Both fluids show high yield stress in response to the applied magnetic field. In the case of hydrocarbon-based MRF-132-AD, yield stress of about 42 kPa at magnetic field intensity of 200 kA/m is achievable [6-8]. In the case of silicon-based MRF-336-AG, yield stress of about 45 kPa at magnetic field intensity of 200 kA/m is achievable [6-8].

Both layouts, valve and orifice, are designed for better comparison in similar packaging.

### 3. MRF valve and orifice parameter calculations

The pressure drop created in the valve mode is the sum of the viscous (purely rheological) component  $\Delta P_r$  and the magnetic field dependent (magneto-rheological) component  $\Delta P_{mr}$ . The value of this pressure drop is defined using the following approximation [3]:

$$\Delta P = \Delta P_r + \Delta P_{mr} = \frac{[12 \cdot \eta \cdot Q \cdot L]}{[g^3 \cdot w]} + \frac{[f \cdot \tau_{mr} \cdot L]}{g} \quad (1)$$

The purely rheological  $\Delta P_r$  term of Eq. (1) is valid for rectangular ducts. The magneto-rheological pressure drop  $\Delta P_{mr}$  is dependent on applied magnetic field. The magnetic field dependent component is the yield stress,  $\tau_{mr}$ , which is developed in response to the applied magnetic field. In the viscous component in this equation  $\eta [Pa \cdot s]$  is the dynamic viscosity,  $Q [m^3/s]$  is the flow rate and  $L, w, g [m]$  are the geometric length, width and gap size of the flow channel respectively. The relationship between the purely rheological and the magneto-rheological part in the Eq. (1) is complex. Therefore an empirical factor  $f [-]$  (no units) has been introduced. In the case where the magneto-rheological part is the more significant, i.e.  $\Delta P_{mr} / \Delta P_r$  is about 100, this factor is 3 [5]. When the fluid movement is large, purely rheological component of Eq. (1) is most important in determining the pressure drop, and  $f [-]$  must be reduced to the lower value (2 or less). The pressure drop in the rectangular channel caused by fluid flow  $Q [m^3/s]$  through the gap  $g [mm]$  with particular dynamic viscosity  $\eta [Pa \cdot s]$  is defined with the following equation:

$$\Delta p = \frac{12 \cdot \eta \cdot L \cdot Q}{w \cdot g^3} \quad (2)$$

By using Eq. (2), the purely rheological pressure drop in the valve can be calculated. Fig. 6 shows the pressure drop through the valve considering flow rates of interests from 5 cm<sup>3</sup>/s up to 20 cm<sup>3</sup>/s. Eq. (2) and the MRF 132-AD viscosity specification [8] have been used.

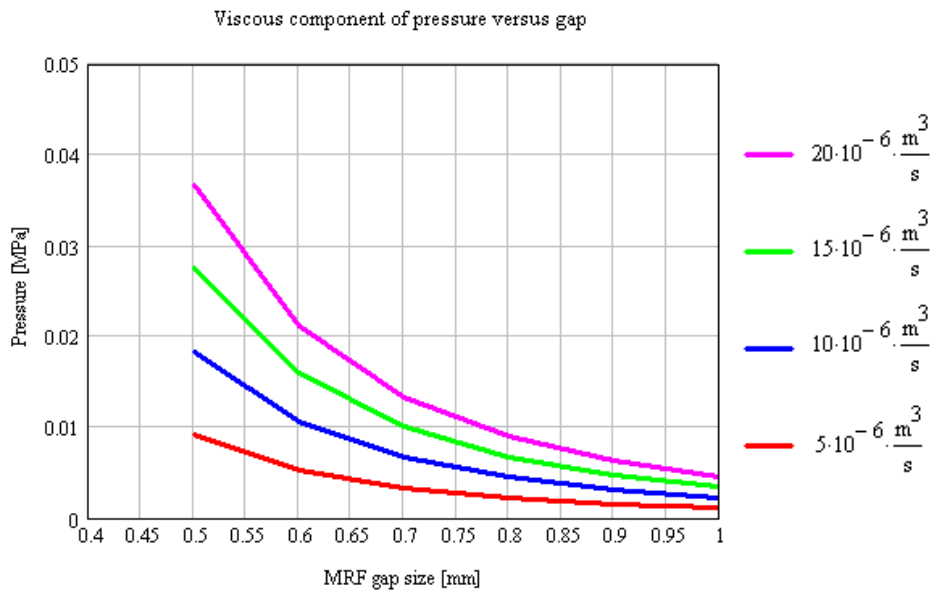


Fig. 6: Pressure versus gap size at various flow rates

For the final design of this study, a number of iterative parameter calculations have been done in order to evaluate the achievable performance. Fig. 7 shows the relationship of achievable magneto-rheological pressure drop in the MRF valve versus the gap size using the yield stress range up to 45kPa. The required magnetic field intensity to achieve the highest yield stress is about 200 kA/m.

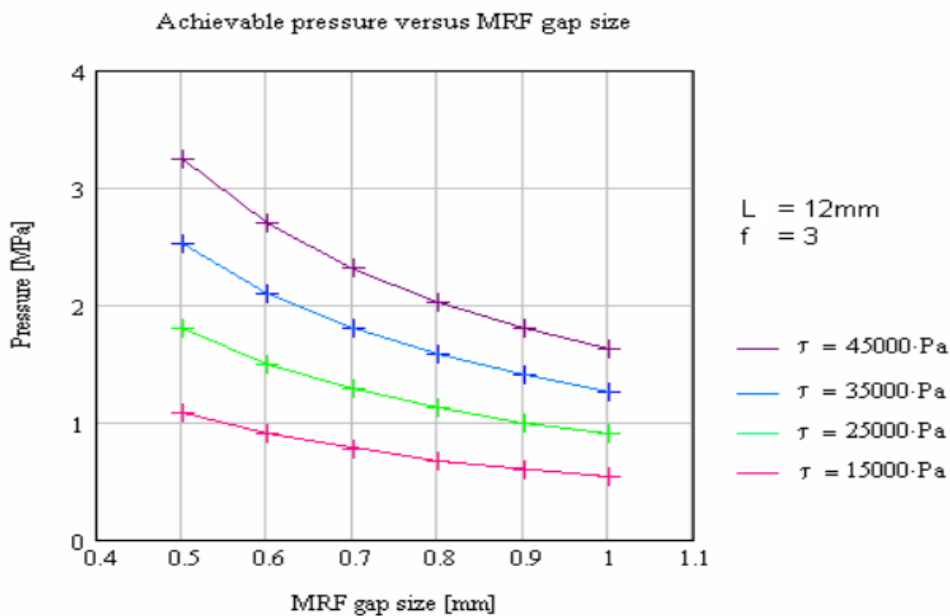


Fig. 7: Pressure drop versus gap size with yield stress as parameter

In this control valve, the magnetic field is perpendicular to the direction of fluid flow. However as alternative to the control arrangement has been proposed and will be evaluated. Fig. 4 depicts the alternative design of the control arrangement which is a controllable orifice. The magnetic field is parallel to the fluid flow in this new proposed orifice mode. The layout of the orifice is simpler and less expensive than for the MRF control valve. To calculate the

pressure capabilities of this orifice arrangement Eq. (1) has to be adjusted for cylindrical shape of the channel.

$$\Delta P = \Delta P_r + \Delta P_{mrf} = \frac{[8 \cdot \eta \cdot Q \cdot L_o]}{\pi \cdot \left(\frac{d_o}{2}\right)^4} + \frac{[f \cdot \tau_{mrf} \cdot L_o]}{d_o} \quad (3)$$

In the viscous component in this equation  $\eta [Pa \cdot s]$  is the dynamic viscosity,  $Q [m^3/s]$  is the flow rate and  $L_o$  and  $d_o [m]$  is the geometric length and the diameter of the flow channel. The factor  $f [-]$  (no units) is an empirical factor. The performance of this arrangement will be evaluated experimentally. The pressure drop in the cylindrical channel caused by fluid flow  $Q [m^3/s]$  with particular dynamic viscosity  $\eta [Pa \cdot s]$  is defined with the following equation:

$$\Delta P_r = \frac{8 \cdot \eta \cdot L \cdot Q}{\pi \cdot r^4} \quad (4)$$

Fig. 8 depicts the pure rheological pressure drop through the orifice considering the flow rate from  $5 \text{ cm}^3/s$  up to  $20 \text{ cm}^3/s$ . Equation (4) for viscous component and the MRF 132-AD specification [8] have been used for calculation.

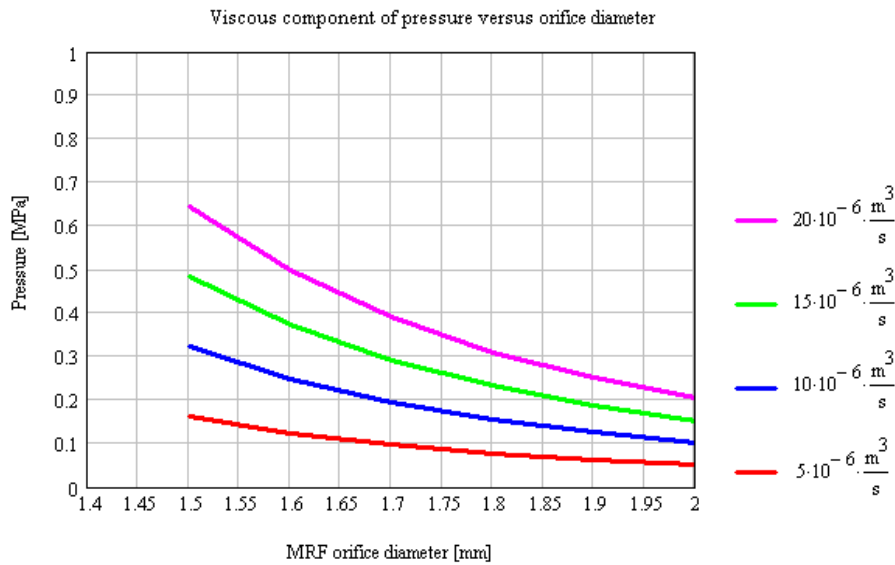


Fig. 8: Pressure versus orifice diameter at various flow rates

Fig. 9 shows the relationship for achievable pressure drop in the MRF orifice versus the orifice diameter using the yield stress range up to 45kPa. The required magnetic field intensity to achieve the highest yield stress is about 200 kA/m. The pure rheological component of Eq. (3) is more significant for the orifice in determining the pressure drop. The factor  $f [-]$  must be set to a lower value (i.e. 1) than in the valve mode.

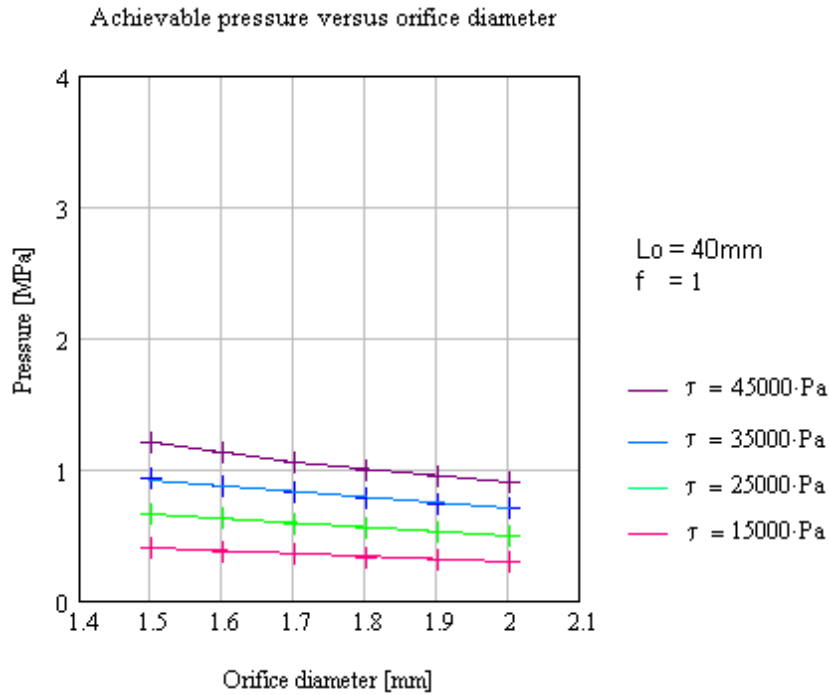


Fig. 9: Pressure versus orifice diameter with yield stress as parameter

From above shown parametrical calculations, it can be concluded that the MR control valve (shown in Fig. 2) is the favorite for this study. This conclusion is based on the fact that the calculations for the valve layout suggest a significantly higher achievable pressure drop than those for the orifice layout. Furthermore, the parasitic pressure causing the fluid to flow in the proposed valve as a result of its low viscosity when the magnetic field is removed is much lower than in the orifice (shown in Fig. 4). Both MRF devices, shown in Fig. 2 and 4, have been designed and prepared for testing on the rig to confirm the basic functionality and the analytical calculations with experimental results. The chosen gap for the valve is about 0.5mm and the chosen diameter of the orifice is 1.5mm. This selection has been based on the results of the parametric calculations.

#### 4. The magnetic circuitry for magneto-rheological devices

A coil in an appropriate ferromagnetic housing needs to be defined as the source of the magnetic field. The magnetic field is the result of electric power flow, current  $I$  [A] and voltage  $U$  [V], through the coil. The coil is wound around the bobbin and the magnetic field is guided through the MRF gap perpendicularly to the fluid flow. All ferromagnetic components, the housing, the internal shaft and the MRF, have to be considered for the evaluation of the magnetic circuitry. For the parametrical calculation it was necessary to perform a trial and error series of operations to find out how many turns the coil needs to have in order to provide the required field strength and how much space this coil will need. To perform these

calculations, layout geometries had to be assumed initially, i.e. the outer diameter of the housing, and then tuned to the optimum. Finally, magnetic field simulation must be used to confirm the magnetic field calculations.

Fig. 10 shows the main magnetic path through the favorite MRF valve arrangement.

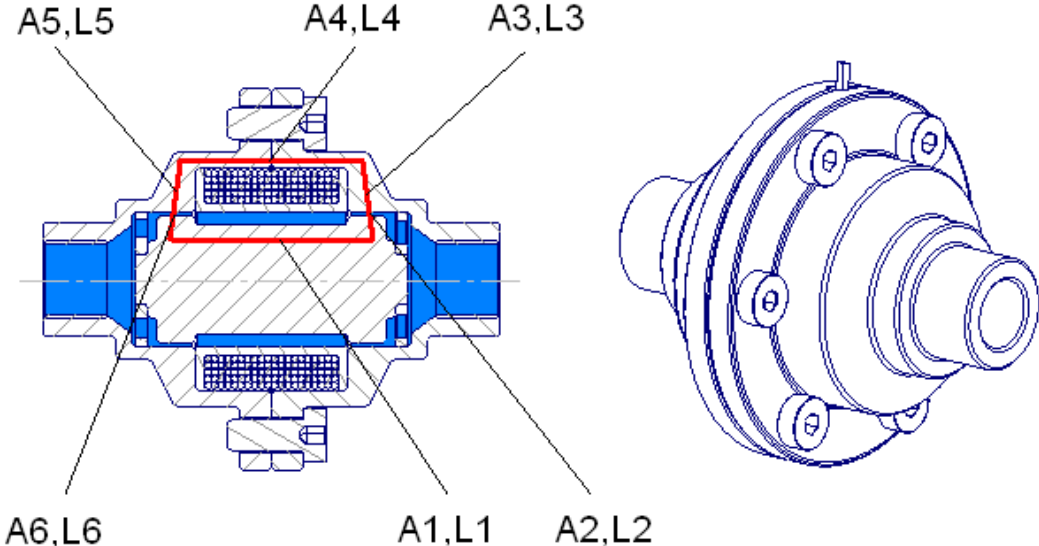


Fig. 10: Magnetic path through the valve

The requirement of the magnetic field strength for the MRF is in the range up to 200kA/m. The alternative arrangement has been introduced in Fig. 4. In this case also a coil in a ferromagnetic housing needs to be defined as the source of the magnetic field. The coil is wound around the bobbin and the magnetic field is guided directly into the MRF, which is in the orifice. The bobbin inner diameter is designed to be only slightly larger than the orifice diameter. The magnetic field direction is inline with the fluid flow direction. Fig. 11 shows the main magnetic path through the alternative MRF orifice arrangement.

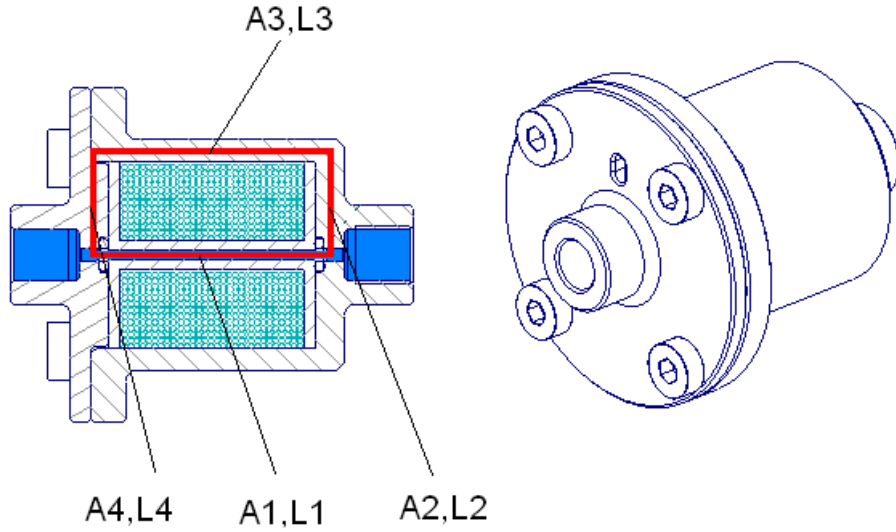


Fig. 11: Magnetic path through the control orifice

For the housing in the valve assembly (favorite) and the orifice (alternative) the low carbon steel, Ck15, has been used. The magnetic property, BH-data, of both MRF132 and MRF 336 have been taken from the MRF supplier [7 and 8]. In order to achieve a fast response it is required to minimize the amount of the ferromagnetic steel in the magnetic circuit. In Fig. 10 and 11 there are several designated sections of component through which the magnetic flux passes. Therefore:

$$\oint H dl_{MRF} = N_{MRF} \cdot I_{MRF} = H_1 \cdot l_1 + H_2 \cdot l_2 + \dots + H_n \cdot l_n \quad (5)$$

Where H is the field strength, l is the gap length and N is number of turns in the coil. Since the flux is constant, the product of flux density and cross-sectional area must be constant for each material:

$$\phi_{MRF} = \phi_{steel} \quad (6)$$

$$B_{MRF} \cdot A_{MRF} = B_{steel} \cdot A_{steel} \quad (7)$$

The flux density B (Tesla) depends on the properties of the material and specially the relative  $\mu_r$  (-) and absolute permeability  $\mu$ . They are sometimes written in the form:

$$B_{MRF} = \mu_0 \cdot \mu_{MRF} \cdot H_{MRF} \quad (8)$$

where  $\mu_0$ , the permeability of free space is constant, and  $\mu_r$ , the relative permeability is another variable with different values for each value of magnetic field strength and for each material. The reluctance,  $\mathfrak{R}$ , is an analog to the resistance in the electric circuit. For the calculation of the reluctance the following equation can be establish:

$$\mathfrak{R} = \frac{MMF}{\phi} = \frac{N \cdot I}{\phi} \quad (9)$$

Where, MMF is the magneto-motive force and  $\phi$  is the flux. The reluctance is sometimes written in the form:

$$\mathfrak{R} = \frac{l}{\mu_0 \cdot \mu_R \cdot A} \quad (10)$$

The total system reluctance can be calculated as follows:

$$\mathfrak{R}_{total} = \mathfrak{R}_1 + \mathfrak{R}_2 + \mathfrak{R}_3 + \dots + \mathfrak{R}_n \quad (11)$$

Ohm's law for magnetic circuit could be formed as:

$$MMF = \phi \cdot \mathfrak{R} \quad (12)$$

In the magnetic path through an assembly, components specific reluctance has to be considered separately:

$$MMF = \phi \cdot (\mathfrak{R}_1 + \mathfrak{R}_2 + \mathfrak{R}_3 + \dots + \mathfrak{R}_n) \quad (13)$$

The inductance (Weber-turns per Ampere) of the magnetic circuit is defined as:

$$L = \frac{N^2}{\mathfrak{R}_{total}} \quad (14)$$

Due to combination of equations (9) with (10), considering equations (6) to (8), following equation can be introduced:

$$N = \frac{\mathfrak{R}_{total} \mu_0 \cdot \mu_{MRF} \cdot H_{MRF} \cdot A_{MRF}}{I} \quad (15)$$

It is now possible to follow a simplified procedure to calculate the required number of turns to achieve the required magnetic field strength. For the parametric calculation, to determine the number turns, the relative permeability of Ck15 and MRF-132-AD have been set as constant. These constants,  $\mu_{Ck15}$  and  $\mu_{MRF-132-AD}$ , have been set to average values for each material based on their B-H properties. Fig. 12 and 13 depict typical results from the calculation for the required number of turns for the valve and orifice design. Other results can be obtained by changing the value of the current.

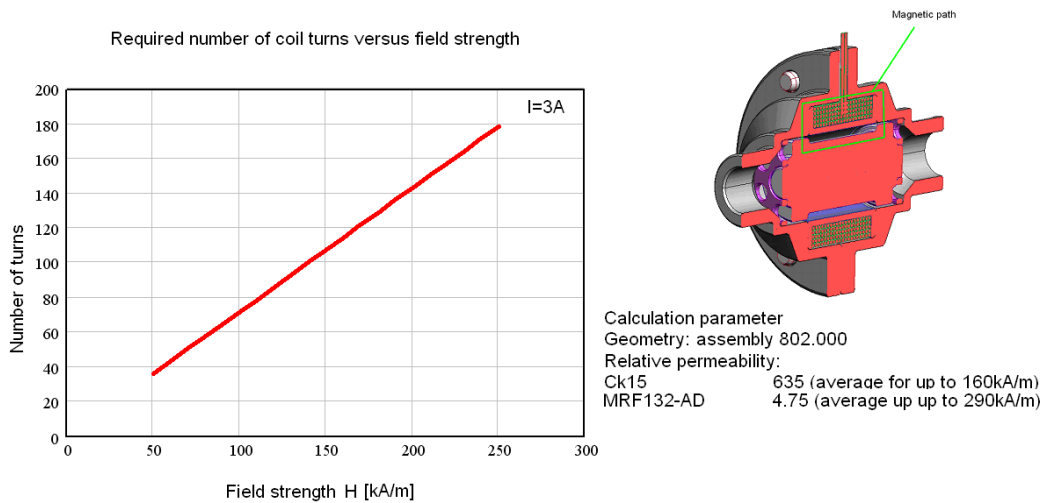


Fig. 12: Number of turns versus achievable magnetic field strength for the valve

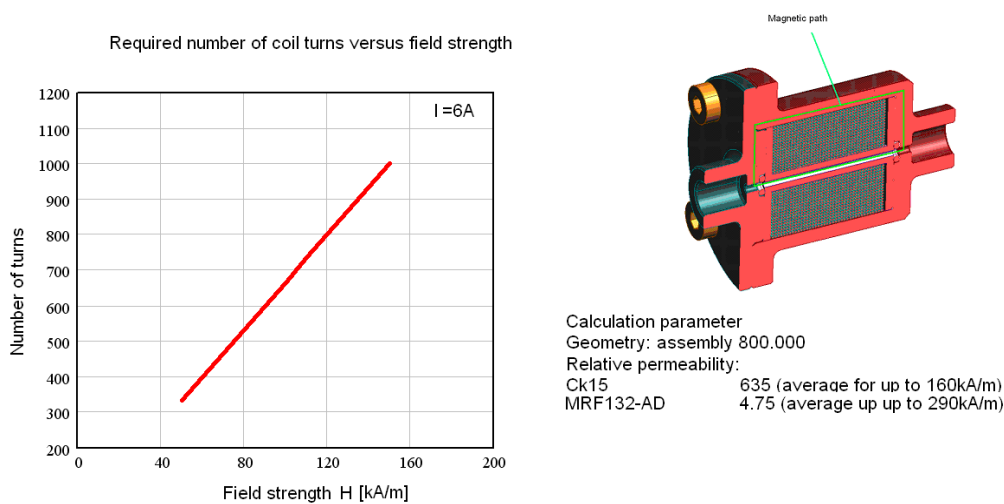


Fig. 13: Number of turns versus achievable magnetic field strength for the orifice

It is again obvious that the valve layout is the preferred layout. These calculations have been prepared as the first input for simulation of the magnetic circuit. The nonlinear B-H characteristics (which leads to relative permeabilities which are not constant) of each material will be used in the magnetic field simulation. The calculation results shown above have been used as the initial input for the magnetic simulation software. Further optimization can then be achieved by running the software programme and making further refinements of the geometry.

## 5. Electric coil for magnetorheological arrangements

Each strand of the copper wire is coated with an insulating layer to avoid electrical short circuits. The insulated wire is about 10% larger than the un-insulated wire. The overall

resistance of the copper wire in the coil can be calculated if the geometry, length and cross-sectional area are known.

$$R_{dc} = \frac{\delta \cdot l_{wire}}{A_{wire}} \quad (16)$$

The resistivity of copper,  $\delta$ , is defined by 0.01786 Ohm·mm<sup>2</sup>/m. There is also a variation of the resistivity of copper with temperature, and this also must be taken into consideration. Over the temperature range of interest:

$$R_{\theta} = R_{20} \cdot (1 + \alpha_{20} \cdot (\theta - 20 \text{ } ^\circ\text{C})) \quad (17)$$

where  $\theta$  is the temperature in degrees centigrade and the temperature constant,  $\alpha$  at 20°C, is defined by 0.0039 1/°C. Fig. 14 shows results of the parametric calculation of current density versus wire diameter. Generally, the limitation is given by thermal conditions and the isolation layer specification for the copper wire.

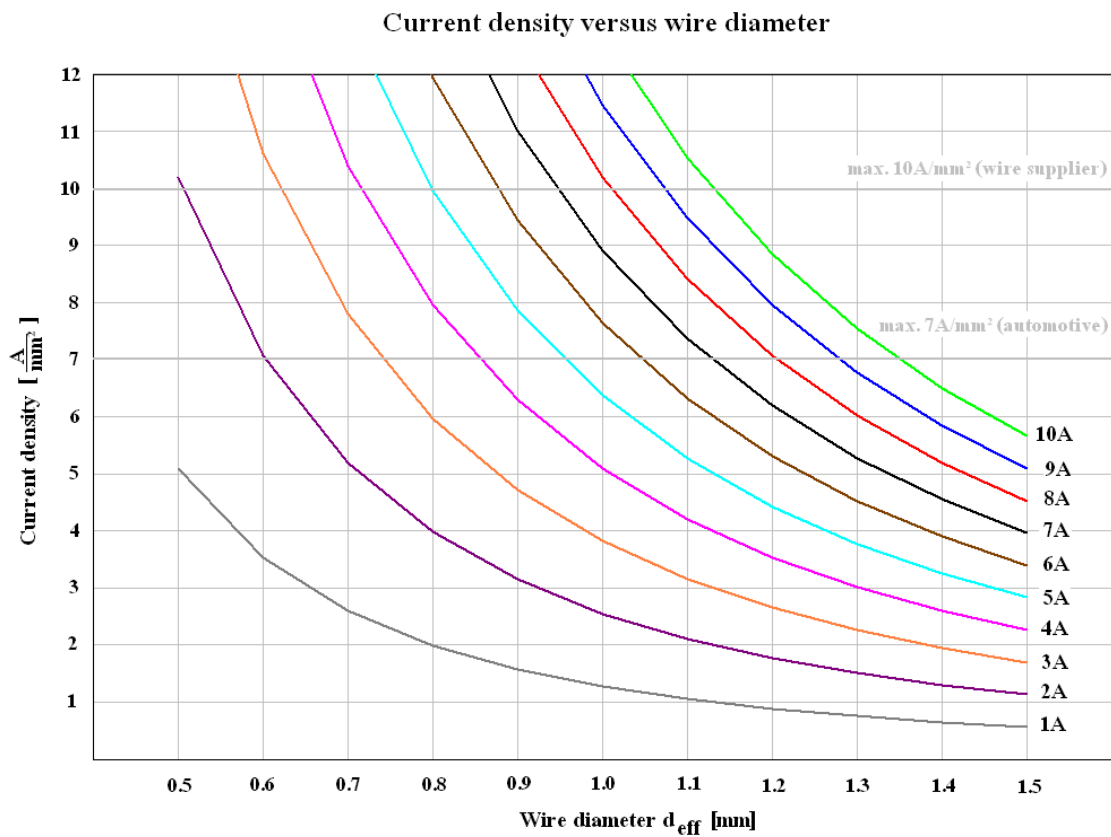
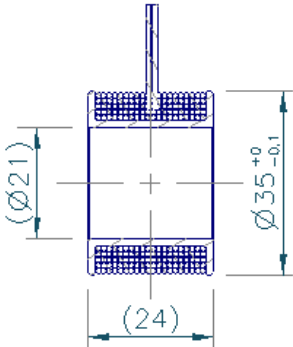


Fig. 14: Current density versus wire diameter with current as parameter

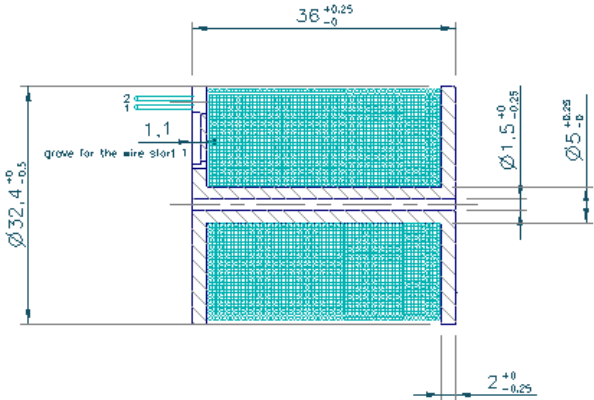
It is now necessary to perform a trial and error series of operations to find out how many turns the coil needs to have in order to overcome the reluctance. The parametrical calculation results, used to specify the prototype coil, have been proven by non-linear magnetic field simulation. Based on above discussed analytical calculations and the results from the

magnetic field simulations, prototype specification for coils has been proposed. Fig. 15 and 16 depict the coil specification of the favorite MRF control valve and the alternative MRF orifice respectively.



Control coil for rig tests  
 Temperature range:  $-20^{\circ}\text{C}$  up to  $+120^{\circ}\text{C}$   
 Supplied voltage:  $2\text{V} \pm 0.5\text{V}$ ,  
 Frequency:  $0\text{Hz}$  at DC and  $1000\text{Hz}$  at AC  
 Resistance at Rt:  $>0.33\text{ Ohm}$  at DC  
 Inductance:  $1\text{mH}$   
 Nominal current:  $<6.2\text{ A}$   
 Number of turns:  $>120$   
 Wire material: Copper  
 Wire bare diameter:  $0.9\text{mm}$

Fig. 15: Geometry and coil specification of the control valve



Control coil for rig tests  
 Temperature range:  $-20\text{ C}$  up to  $+120\text{ C}$   
 Supplied voltage:  $5\text{V} \pm 1.5\text{V}$ ,  
 Frequency:  $0\text{Hz}$  at DC and  $1000\text{Hz}$  at AC  
 Resistance at Rt:  $>0.81\text{ Ohm}$  at DC  
 Inductance:  $8\text{mH}$   
 Nominal current:  $<6.2\text{ A}$   
 Number of turns:  $>510$   
 Wire material: Copper  
 Wire bare diameter:  $0.92\text{mm}$  (AWG19)

Fig. 16: Geometry and coil specification of the control orifice

**6. Magnetic field simulation results from "MR"-valve and "MR"-orifice**

The magnetic field simulation tool FEMM software version 4 has been used for optimization. The simulation problem type has been set up to an “axisymmetric problem”. For the simulation the “asymptotic boundary conditions” have been applied. The non-linear B-H characteristic for each material has been used as input for the magnetic field simulation software. Based on parametric calculations the nominal current for the control coil has been set up to 3 Amperes. For the evaluation of the magnetic circuit voltage drop, flux linkage, inductance, resistance and electrical power have been calculated. Fig. 17 shows the assembly cross-section for 2D-plots for magnitude of field density B (Tesla) and magnitude of field intensity H (A/m) of the mid of MRF gap along defined path line, marked as length. Fig. 18 shows the magnetic flux density plot B (Tesla) of the mid of MRF gap in the valve assembly.

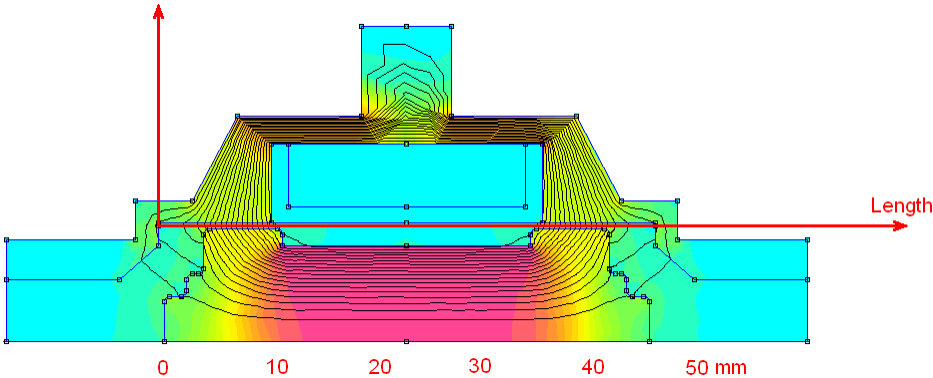


Fig. 17: Reference figure of the valve assembly for plots of B (Tesla) and H (A/m)

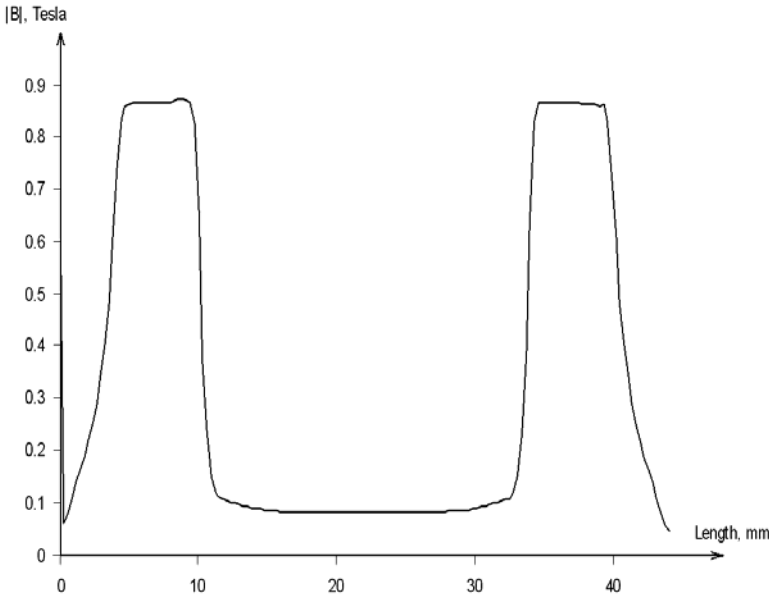


Fig. 18: FEMM Magnetic flux density of B (Tesla) in the valve gap

The geometry of the assembly has been verified up to the homogeneous density of the magnetic field along and across the MRF gap has been achieved and the density level was acceptable. At the magnetic field intensity about 200 kA/m the expected yield stress of MRF

132-AD should be higher than 42kPa. Fig. 19 shows the magnitude of field intensity  $H$  (A/m) related to the mid of the MRF gap.

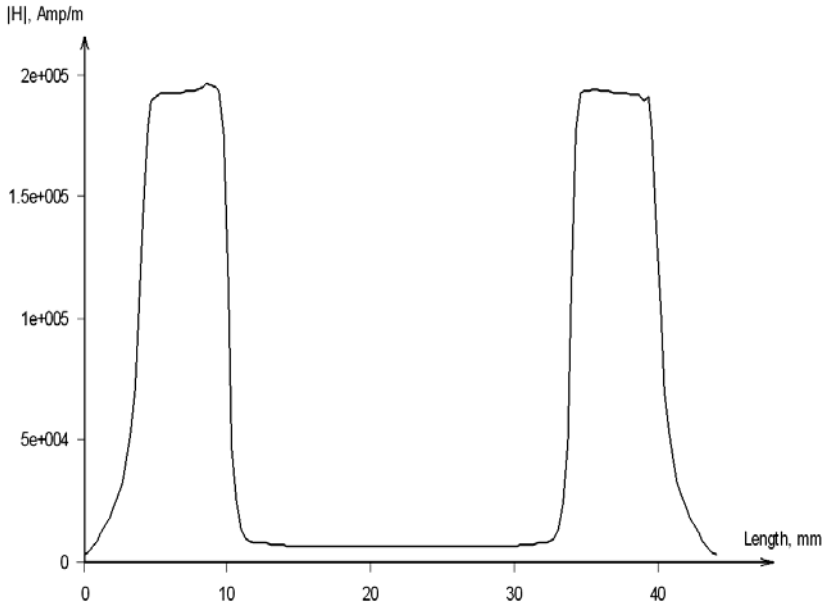


Fig. 19: FEMM Field intensity  $H$  (A/m) in the valve, mid of MRF gap

Also in the orifice layout, for the evaluation of the magnetic circuit, voltage drop, flux linkage, inductance, resistance and electrical power have been calculated. Based on parametric calculations the nominal current for the control coil from the orifice has been set to 6 A. Fig. 20 presents the assembly cross-section for 2D-plots for magnitude of field density  $B$  (Tesla) and magnitude of field intensity  $H$  (A/m) of the mid of MRF orifice along defined path line marked as length. Fig. 21 depicts the magnetic field density plot  $B$  (Tesla) of the mid of MRF orifice.

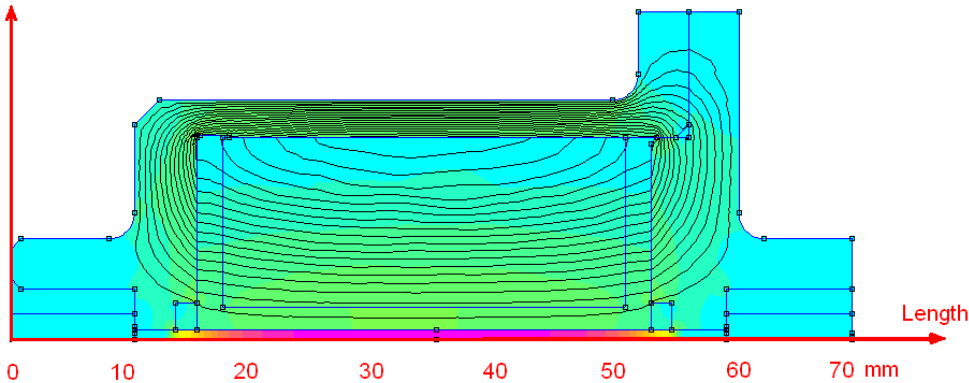


Fig. 20: Reference figure of the orifice for plots of  $B$  (Tesla) and  $H$  (A/m)

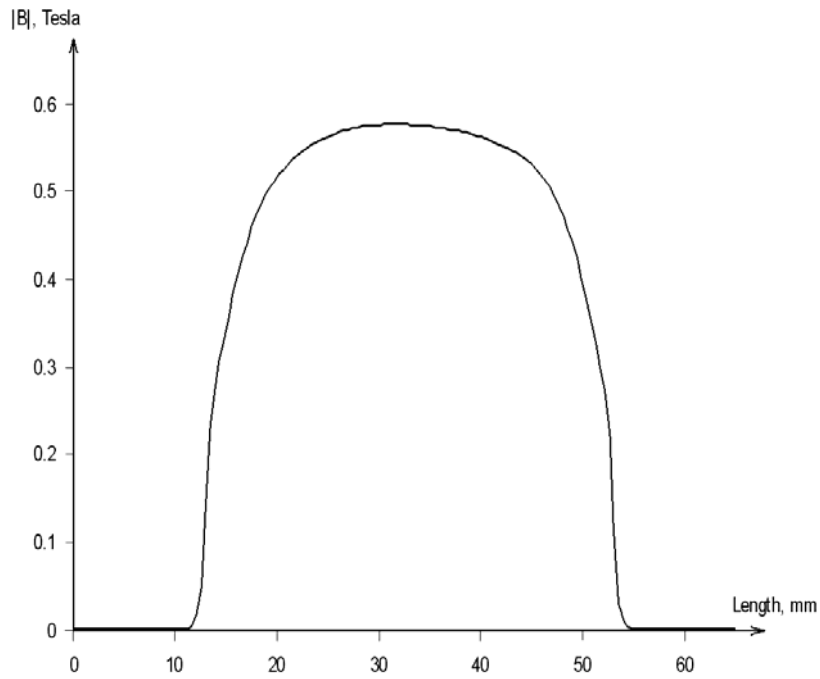


Fig. 21: FEMM Magnetic flux density plot B (Tesla) in the orifice

The geometry of the assembly was tested. At the magnetic field intensity about 95000 A/m the expected yield stress of MRF 132-AD should be about 27kPa. Fig. 22 shows the magnitude of field intensity H (A/m) related to the mid of the MRF orifice.

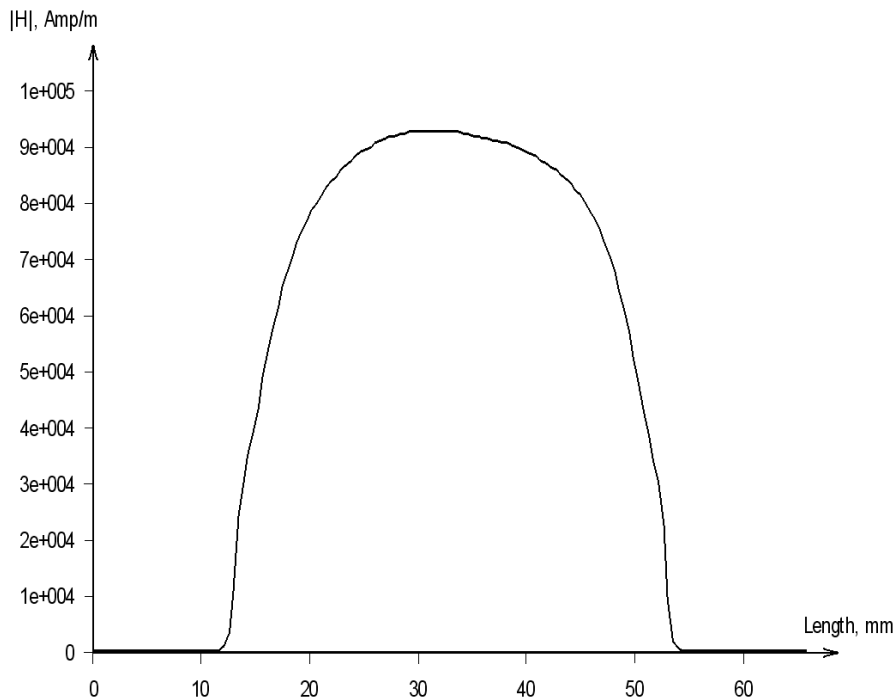


Fig. 22: FEMM Field intensity H (A/m) in the orifice

The orifice assembly is simpler than the preferred control valve assembly. The achievable performance would not be as good as the performance with preferred MRF control valve. An

acceptable distribution of the magnetic field intensity along the MRF orifice has been achieved and the intensity level has been rated as acceptable for the simpler device. The initially proposed geometry, based on analytical calculation, has been optimized with the simulation tool. Several loops of simulations have been obtained before the design freeze for prototyping. The results of the magnetic field simulation have been used to set up the final design for experimental evaluation.

### 7. Experimental evaluation of magneto-rheological control

The assembly of the control valve and orifice are presented in Fig. 23 and 24. The measured weight of the “MR”-valve assembly is 475g and the volume is 70mm<sup>3</sup>. The measured weight of the “MR”-orifice assembly is 530g and the volume is 75mm<sup>3</sup>. Overall packaging and weight of both designs, valve and orifice, have been found as acceptable for comparison of functional performance.



Fig. 23: Picture from “MR”-control valve assembly

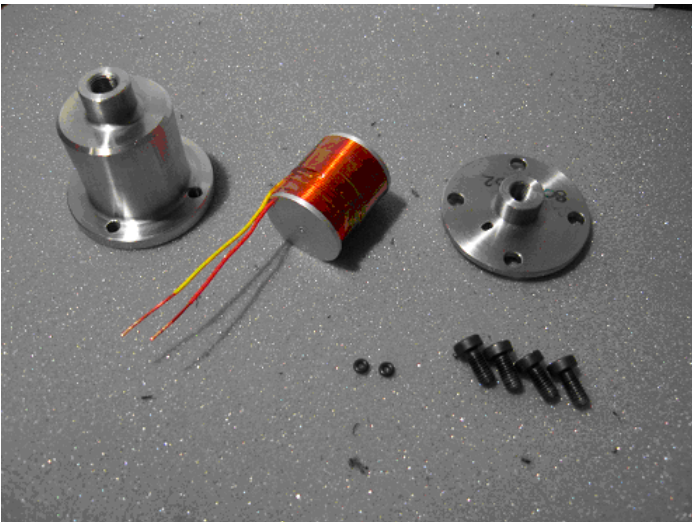


Fig. 24: Picture from control orifice assembly

The static pressure capability versus applied current in the valve or orifice coil has been evaluated. Fig. 25 depicts arrangement together with a cross section of the structure used for experimental tests of the valve assembly. Fig. 26 presents arrangement for experimental tests of the alternative orifice assembly.

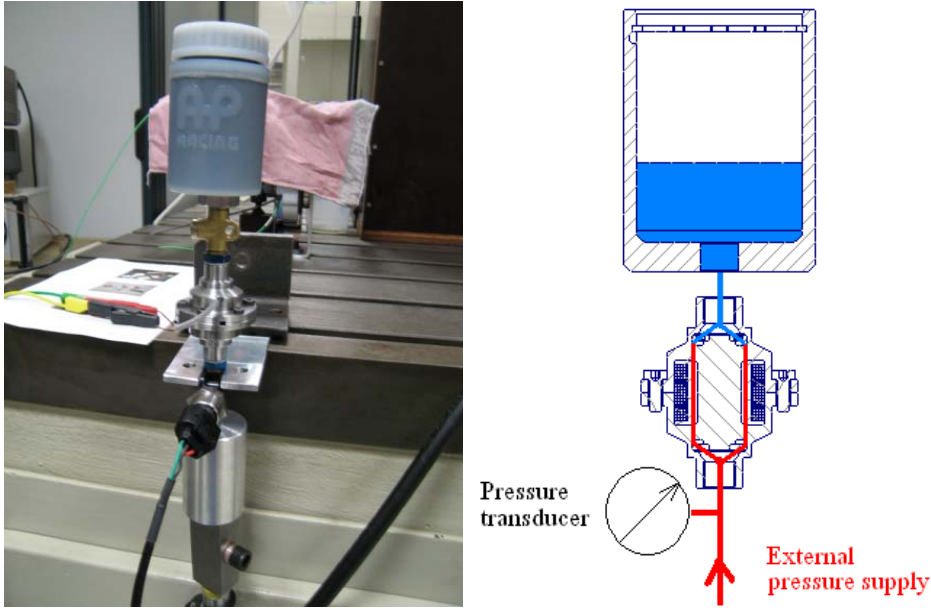


Fig. 25: Layout for experimental tests of the valve

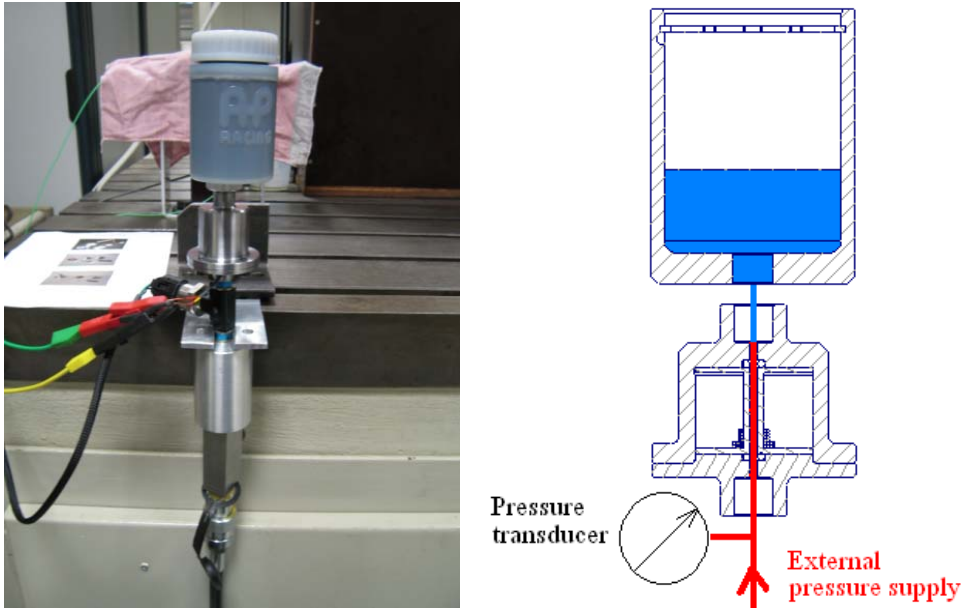


Fig. 26: Layout for experimental tests of the orifice

The position of the reservoir during the testing was chosen to be at the top. An external pump arrangement has been used to bleed the system. Both assemblies have been evaluated with MRF 132-AD and with MRF 336-AG. The external pressure was supplied from a reservoir to the rig equipment; the maximal achievable external flow rate was about  $5 \cdot 10^{-6} \text{ m}^3/\text{s}$ . The pumping through the valve without supply on electrical current to the engaged coil, produced a pressure drop of approximately 0.05 MPa. The experimental evaluation was carried out at

an ambient temperature of +20°C. The silicon based fluid was found to be challenging for conventional bleeding and sealing devices. The MRF 336-AG fluid behavior in the orifice control arrangement, as well in the valve control arrangement, was found to be less satisfactory and less predictable compared with MRF 132-AD. Generally, silicon based MRF's are more difficult to seal and to bleed compared with hydrocarbon based MRF's. On the other hand, silicon based MRF's are less sensitive to temperature variation. To help with the bleeding procedure, the fluid was heated up to about +60°C. Good bleeding is essential for predictable experimental results. The recorded data from the experimental evaluation of the orifice and the valve assemblies, with MRF 132 and MRF 336, are depicted in Fig. 27.

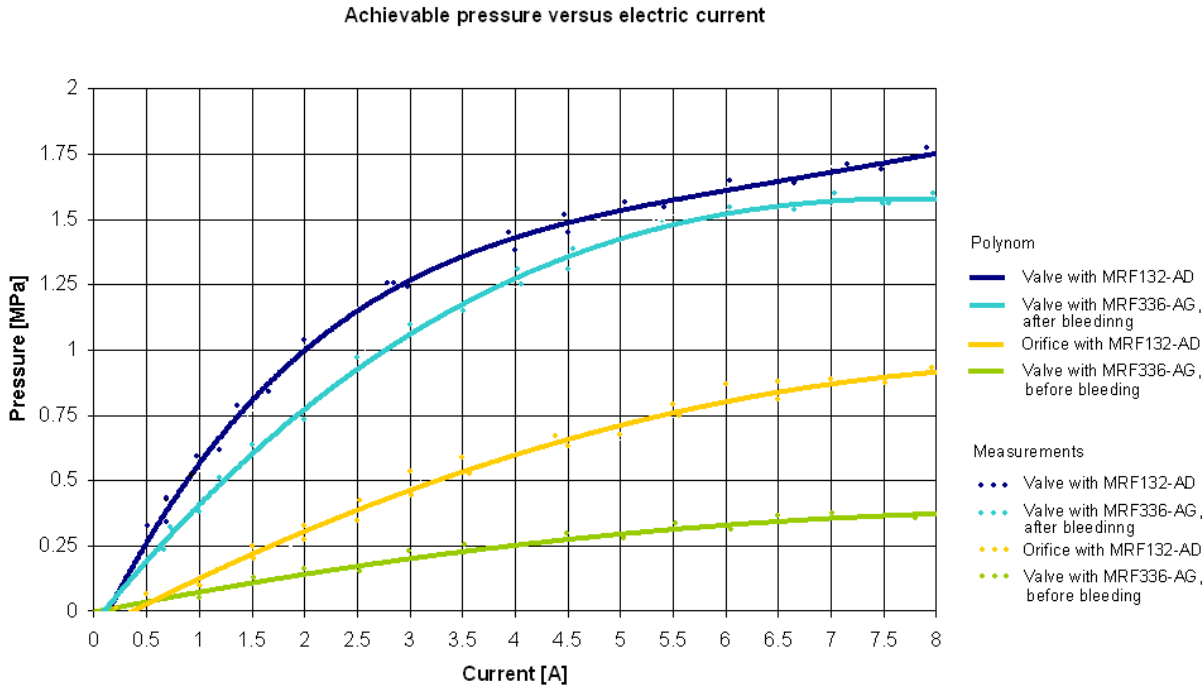


Fig. 27: Pressure capacity of MRF control assemblies

The pressure drop of the “MR”-orifice depends strongly on flow rate. Non homogeneous magnetic field density along and across the orifice causes a chain-like structure of MRF particles, which is not orthogonal to the fluid motion. A continuous flow rate of 5cm<sup>3</sup>/s was required to achieve pressure drop in the orifice. On the other side, the “MR”-valve was capable to hold the pressure without a significant leakage. In the valve gap, the magnetic field is homogeneous and causes orthogonal alignment of the chain-like structure of MRF particles to the fluid motion. The achievable pressure drop in the valve is much higher than in the orifice. It was concluded from the experimental results that the preferred control structure is the “MR”-valve, and the preferred fluid for the test is MRF 132-AD. Based on achieved results it can be stated that magneto-rheological technology offers big potential for various fluid applications.

One of these possible applications could be a pressure release valve. A reference load assembly, hydraulic piston working against a disc spring, has been prepared for evaluation of the pressure release behavior. The reference load assembly represents the elasticity of a typical clutch mechanism. The assembly, used for experimental evaluation, is presented in Fig. 28. The cross-section of experimental rig is shown in Fig. 29.



Fig. 28: Experimental rig load assembly

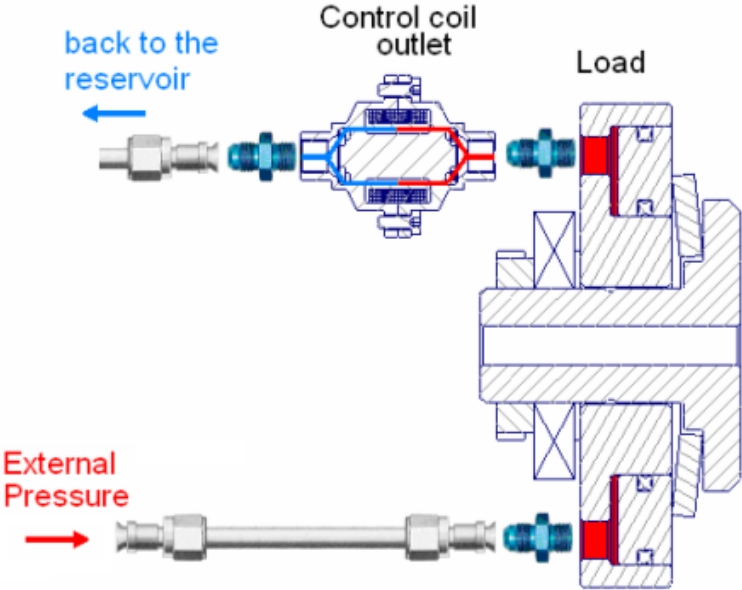


Fig. 29: Layout for experimental tests of the load assembly

The dis-engagement performance has been evaluated experimentally. Axial force, hydraulic pressure and axial displacement have been recorded. Figure 30 and 31 present the dis-engagement performance (pressure release) of the “MR”-valve within the reference assembly from high and from low pressure levels.

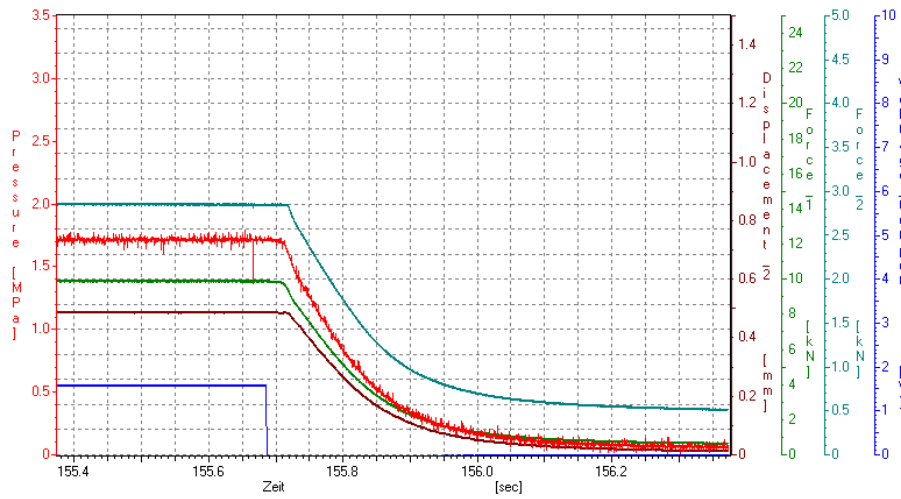


Fig. 30: Disengagement performance from 1.7MPa to 0

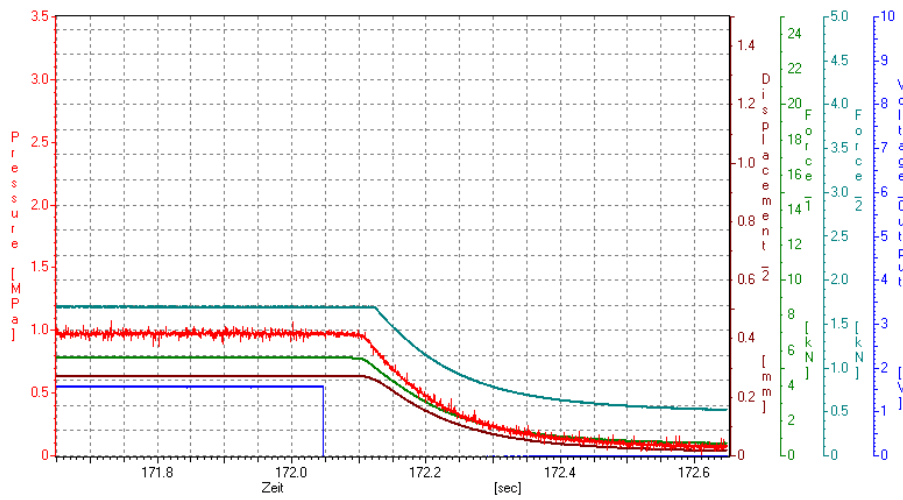


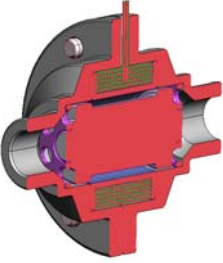
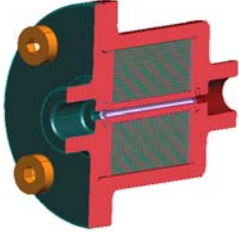
Fig. 31: Disengagement performance from 1.0MPa to 0

In this experimental evaluation the de-activation time was evaluated. Some delay, up to 25ms, has been obtained by conditioning of the signal from analog format to digital format. Less than 150ms were required to decrease the pressure from 1.0MPa to 0.25MPa, and about 200ms were required to decrease the pressure from 1.7MPa to 0.25MPa.

## 8. Conclusions

A literature survey for “MR”-technology [15] has been extended with analytical calculations, magnetic field simulations and an experimental evaluation on a rig. Based on calculations and simulation results, designs of control components based on the “MR”-technology have been developed. Experimental rig assemblies of two different control arrangements have been built and the performances have been evaluated experimentally. The key experimental results, related to “MR”-valve and orifice, are summarized in Table 1.

Tab. 1: “MR”-valve and orifice

“MR”-device, 3D CAD cut view	Actuator key data	Experimental results
Valve 	Valve coil: -120 turns, 0.3 Ohm -wire diameter of 0.9 mm MRF gap size: -gap of 0.5mm and -gap length of 12mm	Used fluid: -MRF132-AD Pressure drop at 5cm <sup>3</sup> /s: -less than 0.05MPa Achieved pressure: 1.5MPa @ 4.5A & 0 cm <sup>3</sup> /s
Orifice 	Orifice coil: -490 turns, 0.84 Ohm -wire diameter of 0.9 mm MRF orifice size: -diameter of 1.5mm -length of 40mm	Used fluid: -MRF132-AD Pressure drop at 5cm <sup>3</sup> /s: -less than 0.2MPa Achieved pressure: 0.6MPa @ 4.5A & 5 cm <sup>3</sup> /s

Higher pressure capacity could be achieved using the valve structure with faster control response and less leakage. Presented calculations, magnetic field simulations and experimental evaluation results for both control arrangements, can be used as a basis for future development work. The contactless nature of fluid control and simple "MR"-device structure are attractive for various control devices. However, settling behavior and further improvement of the response time should be evaluated in collaboration with a fluid supplier in the near future.

## Reference list

- [1] H. Janocha (ed.), F. Claeysen, **Adaptronics and Smart Structures**, Springer Verlag, ISBN 3-540-61484-2, 1999, pp. 124-143
- [2] H. Janocha (ed.), **Actuators**, Springer Verlag, ISBN 3-540-61564-4, 2004, pp. 277-292
- [3] Phillips, R.W., **Engineering Applications of Fluids with a Variable Yield Stress**, Thesis, 1969
- [4] J.D. Carlson, **What Makes A Good MR Fluid**, 8<sup>th</sup> International Conference on Electrorheological (ER) and Magnetorheological (MR) Suspensions, Journal of Intelligent Material Systems and Structures, No. 13, 2002, pp. 431-435
- [5] J.D. Carlson, D.M. Catanzarite and K.A.St. Clair, **Commercial Magneto-Rheological Fluid Devices**, Proceedings of the 5th International Conference on ER Fluids, MR Fluids and Associated Technology, 1995, pp. 20-28 and [www.literature.lord.com/root/other/rheonetic/](http://www.literature.lord.com/root/other/rheonetic/)
- [6] M.R. Jolly, J.W. Bender and J.D. Carlson, **Properties and Applications of Commercial Magnetorheological Fluids**, SPIE 5th Annual Int. Symposium on Smart Structures and Materials, 1998, [www.literature.lord.com/root/other/rheonetic/](http://www.literature.lord.com/root/other/rheonetic/)
- [7] Lord Corporation, **Dr. Dave's Do-It-Yourself MR Fluid, Designing with MR Fluid, Magnetic Circuit Design, FAQs, Fluid specifications**, 2006, [www.lord.com](http://www.lord.com)
- [8] J.D. Carlson, Lord Corporation, MRF Workshop in Carry, 2004, workshop hand outs
- [9] P.L. Wong, W.A. Bullough, C. Feng, S. Lingard, **Tribological performance of magnetorheological suspensions**, Wear 247, 2001, Page 33-40
- [10] J. Huang, J.Q. Zhang, Y. Yang, Y.Q. Wei, **Analysis and design of a cylindrical magnetorheological fluid brake**, Journal of Materials Processing Technology, Vol. 129, No. 1, 2002, P 559-562
- [11] J. Rabinow , **Magnetic fluid clutch**, Technical News Bulletin, National Bureau of Standards, 32/4, 1948, pp. 54-60
- [12] W. Wislow, **Field Responsive Fluid Couplings**, US Pat. No. 2.886.151, 1959
- [13] F.D. Goncalves, J.-H. Koo, M. Ahmadian, **A Review of the State of Art in Magnetorheological Fluid Technologies**, The Shock and Vibration Digest, Vol. 38, No. 3, 2006, pp. 203-219
- [14] D. Meeker, FEMM-Software Manual, **Finite Elements Method Magnetics User's Manual and Tutorial**, 2004, [www.feem.com](http://www.feem.com)
- [15] A. G. Olabi, A. Grunwald, **Design and application of magneto-rheological fluid**, Materials & Design, Vol. 28, No. 10, 2007, pp2658-2664.